pollutants

MDPI

Article

Impact of Heavy Metal Contamination on Physical and Physicochemical Characteristics of Soil near Aurubis-Pirdop Copper Smelter in Bulgaria

Milena Kercheva [1,*], Patrycja Boguta [2], Kamil Skic [2], Viktor Kolchakov [1], Katerina Doneva [1] and Maya Benkova [1]

[1] Department of Physics, Erosion, Soil Biota, Institute of Soil Science, Agrotechnologies and Plant Protection "N. Poushkarov", Agricultural Academy, 1331 Sofia, Bulgaria; v.kolchakov@issapp-pushkarov.org (V.K.); k.doneva@issapp-pushkarov.org (K.D.); majaben@abv.bg (M.B.)

[2] Institute of Agrophysics, Polish Academy of Sciences, Doświadczalna 4 Str., 20-290 Lublin, Poland; p.boguta@ipan.lublin.pl (P.B.); kskic@ipan.lublin.pl (K.S.)

* Correspondence: m.kercheva@issapp-pushkarov.org

Abstract

Soil contamination with heavy metals (HM) poses a risk to human health and can impact different soil functions. This study aimed to determine the influence of heavy metal pollution on the physical and physicochemical characteristics of the two profiles of alluvial–deluvial soil under grassland located at different distances from the Aurubis-Pirdop Copper smelter in Bulgaria. Data for soil particle-size distribution, soil bulk and particle densities, mineralogical composition, soil organic carbon contents, cation exchange properties, surface charge, soil water retention curves, pore size distribution—obtained by mercury intrusion porosimetry (MIP)—and thermal properties were obtained. The contents of Pb, Cu, As, Zn, and Cd were above the maximum permissible level in the humic horizon and decreased with depth and distance from the Copper smelter. Depending on HM speciation, the correlations are established with SOC and most physicochemical parameters. It can be concluded that the HMs impact the clay content, specific surface area, distribution of pores, and the water stability of soil aggregate fraction 1–3 mm to varying degrees.

Keywords: soil heavy metal pollution; soil structure; soil physical quality indicators; water stability of soil aggregates; physicochemical properties; soil thermal properties; alluvial-deluvial soil; copper smelter; Pirdop; Bulgaria

check for updates

Academic Editor: Mauro Marini

Received: 30 June 2025
Revised: 18 August 2025
Accepted: 12 September 2025
Published: 1 October 2025

Citation: Kercheva, M.; Boguta, P.; Skic, K.; Kolchakov, V.; Doneva, K.; Benkova, M. Impact of Heavy Metal Contamination on Physical and Physicochemical Characteristics of Soil near Aurubis-Pirdop Copper Smelter in Bulgaria. *Pollutants* **2025**, *5*, 33. https://doi.org/10.3390/pollutants5040033

Copyright: © 2025 by the authors. Licensee MDPI, Basel, Switzerland. This article is an open access article distributed under the terms and conditions of the Creative Commons Attribution (CC BY) license (https://creativecommons.org/licenses/by/4.0/).

1. Introduction

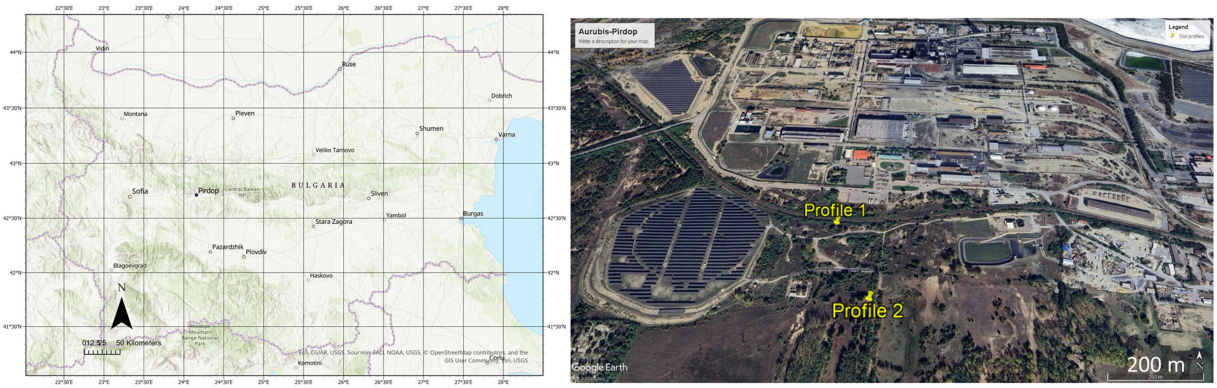
Heavy metal (HM) contamination of soil poses a threat to human health. Numerous studies have been conducted to determine HM distribution, sources, transformations in soil, effects on the environment, and remediation techniques [1–7]. Due to their resistance to degradation, HMs can accumulate in the soil for long periods of time if plants do not absorb them or if they are not moved through runoff, leaching, or flooding during extreme rainfall [7,8]. Factors influencing the accumulation of HMs in soil are soil pH, soil texture, organic matter content, cation exchange capacity (CEC), and soil microbial activity [7]. Acidification increases the mobility of different metals in soil at different rates [6,7,9]. High contents of clay and organic matter in soil contribute to the retention of HMs [6,7]. The impact of HMs on soil quality and ecosystem functions depends on the metal species [6,7] and their complex interactions with minerals, organic matter, microorganisms,

and associated complexes [10]. An experimental study showed that the increase in HM concentrations can decrease clay content and change the pore size and permeability [11]. The type of land use influences soil aggregate size distribution and soil aggregate-associated heavy metals [12]. The Aurubis Bulgaria Copper smelter and refinery is located in Pirdop, and it is the biggest copper facility in Southeast Europe, founded in 1958 [13]. Most of the research conducted in this region monitored the spread of aerosol pollutants and remediation activities [13–15]. There are no investigations into the impact of heavy metal pollution on both structural and physicochemical properties of the soil in the region. In studies conducted over 25 years ago in this area [16], no statistically significant differences in mechanical composition, pH, and humus content as a result of aerosol emission pollution were found. While most of the studies focused on the surface soil layers, the current one explores the distribution of HMs in depth of soil profile. The changes in physical conditions of the contaminated soil are important for assessing the potential risk for groundwater and surface water pollution.

The current study aims to evaluate the physical and physicochemical properties of the acidic alluvial–deluvial soil in the region of the Aurubis Bulgaria Copper smelter in relation to heavy metal concentrations.

2. Materials and Methods

The Aurubis Copper smelter in Pirdop is located in Zlatitsa-Pirdop Valley, surrounded by the Balkan Mountains and the Sredna Gora Mountains in West Bulgaria (Figure 1a). The relief of the valley is flat with a slight southern inclination. The region is covered with grass, shrubs, and sparse deciduous groves. The investigations into the sources of HM contamination in the region [13,16] show that the main mechanism is the aerosol transport from the plant. Two profiles of alluvial–deluvial soil, located at different distances from the smelter, were investigated. Profile 1 (24.1585 E; 42.7117 N, 712 m a.s.l.) is located at a distance of 1000 m from the pollution source, and Profile 2 (24.1596 E; 42.7096 N; 709 m a.s.l.) is located at a greater distance—1300 m (Figure 1b). Soil samples (in undisturbed and disturbed states) were taken from the A horizon at three depths (0–5, 10–15, and 25–30 cm) and from deeper soil layers (40–60 and 60–80 cm, only in disturbed states).



(**a**) (**b**)

Figure 1. Location of the Aurubis Copper smelter in Pirdop (**a**) and the soil profiles (**b**).

The undisturbed soil cores taken with 100 cm^3 metal rings were used to determine the soil bulk density and water retention at suction −0.25 kPa (pF 0.4) on a sand bath, and at −1, −5, −10, and −33 kPa (pF 1, 1.7, 2.0, and 2.5), using a suction-type apparatus (Shot filters G5 (DWK Life Sciences, Mainz, Germany) with diameters of pores 1.0–1.6 µm) as described in [17]. The water retentions at the matric potentials of pF 4.2 (−1500 kPa)

(wilting point) and pF 5.6 (hygroscopic moisture content) were determined using fine (<2 mm) earth samples, correspondingly with a pressure membrane apparatus and the vapor pressure method at 75% relative air humidity in a desiccator, containing a saturated solution of NaCl.

The particle-size distribution was determined by sieving and the pipette method [18]. Particle density (Ds) was determined in water by pycnometers. The distribution of dry aggregates was determined in size classes (>10, 10–5, 5–3, 3–1, 1–0.25, <0.25 mm) by the manual sieving of air-dried soil using a set of sieves [17]. The water stability of aggregates was determined by the Savinov method, with modification by Vershinin and Revut [19]. Four soil samples were analyzed by this method. The composite sample ($F_{0.25–10}$) was prepared by taking an equal quantity (5 g) of air-dried aggregates from four fractions, 10–5, 5–3, 3–1, and 1–0.25 mm. The single aggregate fraction of the 1–3 mm size ($F_{1–3}$) was used to prepare three replicate samples (20 g each) which allows the performance of statistical comparison. Wet sieving was performed using a Savinov device [19] an hour after the direct immersion of the air-dried soil aggregate sample into water (slaked pretreatment). The correction for aggregate-sized sand content was performed as described in [20]. The water stability of aggregates is expressed by the ratio (MWDR) of mean weight diameters of aggregates before and after wet sieving.

The soil thermal properties: Thermal conductivity, thermal diffusivity, and volumetric heat capacity were determined with a KD2Pro device (Decagon Devices, Inc., Pullman, WA, USA) in the soil cores at matric potentials from −0.25 to −33 kPa, drained by the suction-type apparatus, and then air dried by evaporation. The relations of thermal properties with water content were approximated with the de Vries model [21]. The performance of the models was estimated by the root mean square error (RMSE).

The content of total organic carbon (SOC, %) was determined using the modified Tyurin method [22,23]. Soil acidity (pH) was determined in a soil–water suspension of a 1:2.5 ratio.

The physicochemical properties of the soil were determined at the ISSAPP "N. Poushkarov" by the method of Ganev and Arsova [24]: cation exchange capacity ($T_{8.2}$≡CEC) and its constituent shares of strongly acidic (CEC_{SA}) and weakly acidic (CEC_A) positions of the soil adsorbent, total acidity ($H_{8.2}$), exchangeable acidity (exch. Al), exchangeable bases (Ca^{2+}, Mg^{2+}), and degree of saturation with bases (BS). The samples were also analyzed by potentiometric titration to determine the total negative surface charge (Q_v), the charge increment, and the distribution function of the dissociation constant of negatively charged functional groups at pH from 3 to 10 [25]. The titration was performed with a Titrino 702SM (Metrohm, Herisau, Switzerland) apparatus. The aqueous solutions of all soil samples prepared in 0.1 M NaCl were titrated under N_2 atmosphere with 0.1 M NaOH based on 0.1 M NaCl. The analyses were performed in triplicate.

Mercury intrusion porosimetry was determined in triplicate within the range from 0.003 to 360 μm using an Autopore IV 9510 mercury porosimeter (Micromeritics, Norcross, GA, USA). The equivalent pore diameter was estimated from Washburn's equation:

$$D = (-4\sigma_m \cos\theta_m)/P \quad (1)$$

where D is the pore diameter for cylindrical pores, θ_m is the mercury contact angle (assumed 130 degrees), σ_m is the mercury surface tension (0.485 $J \cdot m^{-2}$), and P is the external pressure (Pa). The total pore volume (V_t, $cm^3 \cdot g^{-1}$), total pore area (S_{MIP}, $m^2 \cdot g^{-1}$), and average pore diameter (D_{av}, nm) were calculated from the obtained pore size distributions. The differential curves obtained by mercury intrusion porosimetry were used to analyze diverse pore classes in the following diameter range: macropores (>75 μm), mesopores (75–30 μm),

micropores (30–5 μm), ultramicropores (5–0.1 μm), cryptopores (0.1–0.007 μm), and pores < 0.007 μm [26].

Nitrogen adsorption was measured in two replications on a 3Flex device (Micromeritics, Norcross, GA, USA). The measurement of the amount of gas adsorbed over a range of stepwise increasing partial pressure gave the adsorption isotherm from which the specific surface area (SSA, $m^2 \cdot g^{-1}$) was estimated within the range from 0.05 to 0.35 of relative pressure. The BET model was adopted to estimate SSA, assuming a cylindrical pore shape and that the nitrogen molecule had an area of 0.162 nm^2 at 77 K.

The surface fractal dimensions were calculated from measured desorption isotherms, basing on the Frenkel–Hill–Halsey (FHH) equation. According to this approach, the experimental adsorption, a, was approximated using the following equation:

$$\ln(a) = -(1/m)\ln(-\ln(p/p_0)) + C \quad (2)$$

where C is a constant, and the parameter 1/m is related to the surface fractal dimension of the sample. Experimental data taken for calculations came from the multilayer adsorption region, i.e., for rather high relative pressures where the effects of energetic surface heterogeneity on adsorption may be neglected.

As, Cd, Cu, Pb, and Zn contents were determined with an ICP Optical Emission Spectrometer Series 715-ES (© Agilent Technologies, Inc., Mulgrave, Victoria 3170, Australia) by decomposition with "aqua regia". The content of heavy metals was assessed according to the threshold concentrations for pastures [27,28] and according to a three-level pollution scale [29] and the higher guideline values of the Finnish legislation for contaminated soils [30] considered as "a good approximation of the mean values of different national systems in Europe" [3].

The mineralogical composition was determined by X-ray structural analysis with a D2 PHASER diffractometer (Bruker, Berlin, Germany) on individual samples, after preliminary removal of organic matter with peroxide and separation of two fractions—sand (particles > 63 μm) and silt + clay (<63 μm).

The descriptive statistical analyses and correlation analyses between HMs and the studied soil properties were performed using STATGRAPHICS Centurion 18 software and Excel. The one-way analysis of variance (ANOVA) with post hoc analysis (HSD Tukey test) was used. The tests were carried out taking into account all layers of the two soil profiles. The significance level was estimated at $\alpha = 0.05$.

3. Results and Discussion

The maximum permissible concentrations (MPCs) that apply to pastures and meadows and for soil pH below 6 are presented in Table 1. The Pb, Cu, As, and Cd content in the 0–5 cm surface layer is above the MPC in both profiles. The concentration of these elements in the 0–20 cm surface layer is in the range obtained from another survey in the region [13], except for the higher concentration of Cd and the extremely high value of Pb in the 0–5 cm surface layer of Profile 1. The latter is possible due to the presence of lead ore particles. The concentrations of heavy metals decrease with depth in the soil profiles, as well as with distance from the source of pollution. This phenomenon can be explained by the role of the organic matter in forming HM organic complexes due to the abundant active groups on their surfaces [10]. This mechanism of immobilization of HM is well exhibited in the remote Profile2, where the loading from aerosol pollution is lower.

Excessive Cu concentrations are found in the studied 0–80 cm layer of Profile 1, while in Profile 2, the pollution reaches a depth of 15 cm. The values of Cu exceed even the intervention concentrations (ICs) for industrial sites in both profiles in the surface layers (0–10 cm). The degree of contamination is assessed as strong up to 30 and 15 cm depth,

in the closer and remote profiles, respectively. Pb and As contamination is also strong in the surface layer 0–5 cm, since the values of both elements exceed the MPC and IC, but it decreases sharply in the lower layer of Profile 1. In Profile 2, moderate contamination with these elements is detected only in the 0–5 cm surface layer. The correlation coefficients between As, Pb, and Zn were high (r = 0.83–0.95) (Table 2) and statistically significant ($p < 0.01$), which is an indication of their common source and common mechanism for their distribution in soil. The correlation of Zn with Cu is also significant ($p < 0.01$), but with As and Pb, it is lower (<0.10). The average concentration of Cd is approximately the same in the two studied profiles (5.2 ± 0.9 and 5.8 ± 1.5 mg · kg^{-1}). It is above the MPC (Table 1) and does not correlate with the concentrations of As, Cu, Pb, and Zn (Table 2), suggesting a different mechanism or source.

Table 1. Content of heavy metals in investigated profiles and within the soil layers. MPC—maximum permissible concentrations; IC—intervention concentrations, according to [27] and higher guideline value according to [30].

Depth, cm	As mg·kg^{-1}	Cd mg·kg^{-1}	Cu mg·kg^{-1}	Pb mg·kg^{-1}	Zn mg·kg^{-1}
MPC (pastures, pH < 6)	30	2	80	90	220
IC	90	12	500	500	900
Higher guideline value	100	20	200	750	400
Profile 1					
0–5	181.6	5.7	1101.6	44,498.9	167.8
10–15	39.9	3.9	1013.0	109.9	112.4
25–30	8.0	6.4	801.4	33.5	95.6
40–60	17.3	4.8	392.9	25.9	103.4
60–80	19.5	5.1	325.7	15.3	93.8
Profile 2					
0–5	68.5	4.9	931.0	115.7	94.7
10–15	17.5	6.6	824.2	47.0	109.1
25–30	18.0	3.7	32.2	14.0	72.2
40–60	20.6	7.3	24.3	20.4	66.8
60–80	19.1	6.6	18.8	9.4	72.4

Table 2. Correlations between heavy metal concentrations. Stars denote confidence level of significance of correlations (single star—90% and three stars—99%).

	As	Cd	Cu	Pb	Zn
As	1				
Cd	−0.06	1			
Cu	0.56 *	−0.15	1		
Pb	0.95 ***	0.06	0.45	1	
Zn	0.83 ***	−0.11	0.79 ***	0.84 ***	1

The mineralogical composition of samples from a depth of 25–30 cm shows a predominance of quartz (36–34%), followed by feldspars and muscovite in the sand fraction (>0.063 mm) (Table 3). In the finer fraction (<0.063 mm), feldspars and muscovite predominate. The clay fraction alone was not separated and studied; however, the presence of montmorillonite in the soil was shown. Clay minerals significantly influence the fixation and migration of HMs within soils as a result of different adsorption processes [10].

The soil texture of the humus layer in the studied profiles is Loam (Table 4). In Profile 1, the finer fraction increases with depth, while Profile 2 is more homogeneous. The lower clay content in the 0–5 cm surface layer of Profile 1 can be attributed to the impact of HMs, as discussed further. The content of organic carbon (SOC) is higher, and the soil

reaction (pH) is lower in Profile 1 over the entire depth compared to Profile 2 (Table 5). Exchange acidity (Exch. Al) is higher in Profile 1. The soils are podzolic according to the criterion pH < 6.0, and the sum of basic cations is less than the capacity of the strong acid ion exchanger (CEC_{SA}) [31]. The cation exchange capacity of the soils indicates that they are moderately colloidal, and according to the predominant clay mineralogy, they are montmorillonite-illite (CEC_{SA} = 85–70% CEC) [31].

Table 3. XRD mineralogical composition of samples (<0.063 mm and >0.063 mm) from 25 to 30 cm.

Minerals	Profile 1		Profile 2	
	>63 µm	<63 µm	>63 µm	<63 µm
Quarz (SiO_2)	35.9	12.6	33.8	26.1
Plagioclase [$(Na,Ca)(Si,Al)_4O_8$]	23.1	13.1	18.9	21.3
K-feldspar ($KAlSi_3O_8$)	7.6	25.8	12.1	11.7
Muscovite {$KAl_2[AlSi_3O_{10}](OH)_2$}	21.9	24.3	25.0	34.6
Amphibol {$Ca2_[Mg_4(Al,Fe)]Si_7AlO_{22}(OH)_2$}	2.9	3.7	3.1	4.6
Chlorite {$[Mg,Al,Fe]_6[Si,Al]_4O_{10}(OH)_8$}	6.9	19.7	6.8	0.2
Montmorillonite [$(Na,Ca)_{0,3}(Al,Mg)_2Si_4O_{10}(OH)_2 \bullet n(H_2O)$]		0.8	0.3	1.5
Calcite ($CaCO_3$)	1.6			

Table 4. Soil texture fractions and classes for two soil profiles and different soil depths.

Sampling Depth, cm	Sand (2–0.063 mm), %	Silt (0.063–0.002 mm), %	Clay (<0.002 mm), %	Texture Class
Profile 1				
0–5	29.6	51.5	18.9	Loam
10–15	28.5	48.5	23.0	Loam
25–30	21.1	51.3	27.6	Clay Loam
40–60	20.3	52.6	27.1	Clay Loam
60–80	22.0	48.7	29.2	Clay Loam
Profile 2				
0–5	25.1	50.0	24.8	Loam
10–15	23.0	50.6	26.4	Loam
25–30	26.7	48.5	24.8	Loam
40–60	24.5	48.5	26.9	Clay Loam
60–80	24.7	48.2	27.0	Clay Loam

Table 5. Chemical and physicochemical soil properties. SOC—soil organic carbon content; EC—electrical conductivity; CEC—total sum of exchange cations; CEC_{SA}—cation-exchange capacity of soil strongly acidic ion exchanger; CEC_A—soil slightly acidic ion exchanger; exch. $H_{8.2}$—total acidity; exch. Al exchangeable acidity; Exch. Ca—soil exchangeable calcium; Exch. Mg—soil exchangeable magnesium.

Sampling Depth cm	SOC	pH	EC,	cmol·kg^{-1}							Base
	%	H_2O	ms·cm^{-1}	CEC	CEC_{SA}	CEC_A	Exch.$H_{8.2}$	Exch. Al	Exch. Ca	Exch. Mg	Saturation, %
Profile 1											
0–5	1.49	4.6	0.042	25.0	18.5	6.5	9.6	3.2	13.5	2.0	61
10–15	0.80	4.3	0.035	21.0	14.4	6.6	10.5	4.0	9.0	1.8	50
25–30	0.73	4.4	0.035	21.2	15.7	5.5	9.2	3.6	10.0	1.8	56
40–60	0.69	4.6	0.021	24.0	18.8	5.2	7.6	1.6	14.6	1.9	68
60–80	0.73	4.9	0.021	24.7	19.5	5.2	6.5	1.0	16.2	2.0	73
Profile 2											
0–5	1.09	4.7	0.042	25.1	17.6	7.5	9.2	1.8	14.0	2.0	63
10–15	0.98	5.0	0.056	23.2	17.8	5.4	6.5	1.1	14.5	1.9	71
25–30	0.46	5.4	0.070	23.0	18.8	4.2	5.0	0.8	15.8	1.9	78
40–60	0.34	5.5	0.098	23.0	19.5	3.5	4.2	0.6	16.5	2.0	81
60–80	0.15	5.7	0.126	23.1	19.9	3.2	3.6	0.3	17.5	2.0	84

The average pore diameter (D_{av}), total pore volume (V_t), and surface fractal dimension (D) decreased with soil depth, while the surface area of pores (S_{MIP}) and specific surface area (SSA) increased (Table 6). D_{av} for Profile 1 ranged from 214.96 to 400 nm, and the total pore area from 7.47 to 12.56 $m^2 \cdot g^{-1}$. In the case of Profile 2, D_{av} values ranged from 205.24 to 329.89 nm, while S_{MIP} ranged from 10.10 to 16.93 $m^2 \cdot g^{-1}$. V_t ranged from 0.18 to 0.22 $cm^3 \cdot g^{-1}$ and was the highest for the upper soil horizons.

Table 6. Characteristics of porous space obtained by MIP. Data represent mean values ± standard deviations. The same upper letter (a–g) means no significant differences between the values at the level of significance $\alpha = 0.05$, one-way ANOVA, and Tukey's HSD test.

Sampling Depth	V_t	S_{MIP}	D_{av}	SSA	D	Macropores	Mesopores	Micropores	Ultramicropores	Cryptoprobes	Pores < 7 nm
cm	$cm^3 \cdot g^{-1}$	$m^2 \cdot g^{-1}$	nm	$m^2 \cdot g^{-1}$		%	%	%	%	%	%
Profile 1											
0–5	0.22 ± 0.01^{cd}	7.47 ± 0.25^{a}	400.00 ± 22.27^{e}	11.41 ± 0.02^{a}	2.66 ± 0.000^{g}	3.86 ± 0.24^{b}	0.60 ± 0.02^{d}	0.92 ± 0.02^{e}	78.85 ± 1.89^{f}	14.44 ± 0.66^{a}	1.34 ± 0.03^{a}
10–15	0.19 ± 0.00^{abc}	8.16 ± 0.20^{ab}	269.52 ± 8.57^{c}	13.07 ± 0.03^{b}	2.65 ± 0.001^{f}	4.13 ± 0.07^{b}	0.48 ± 0.04^{c}	0.34 ± 0.02^{b}	73.95 ± 2.78^{def}	19.48 ± 0.22^{c}	1.62 ± 0.03^{b}
25–30	0.20 ± 0.01^{abcd}	10.27 ± 0.56^{bcd}	232.23 ± 13.97^{abc}	15.06 ± 0.08^{c}	2.61 ± 0.001^{c}	3.17 ± 0.16^{a}	0.30 ± 0.02^{a}	0.28 ± 0.01^{a}	72.79 ± 0.91^{cde}	21.40 ± 0.17^{cd}	2.05 ± 0.03^{c}
40–60	0.20 ± 0.01^{abcd}	12.56 ± 0.39^{de}	220.65 ± 10.05^{ab}	17.62 ± 0.17^{e}	2.59 ± 0.001^{b}	3.90 ± 0.15^{b}	0.47 ± 0.02^{c}	0.46 ± 0.02^{c}	68.76 ± 2.32^{bc}	23.29 ± 0.25^{de}	3.11 ± 0.03^{e}
60–80	0.18 ± 0.02^{a}	11.85 ± 1.09^{cde}	214.96 ± 8.15^{ab}	17.83 ± 0.01^{e}	2.60 ± 0.003^{b}	5.09 ± 0.07^{d}	0.27 ± 0.02^{a}	0.30 ± 0.02^{ab}	66.81 ± 1.85^{b}	24.35 ± 0.44^{e}	3.18 ± 0.07^{e}
Profile 2											
0–5	0.22 ± 0.00^{d}	10.56 ± 0.15^{cd}	322.78 ± 10.40^{d}	16.17 ± 0.13^{d}	2.63 ± 0.003^{d}	4.04 ± 0.15^{b}	0.37 ± 0.02^{b}	0.51 ± 0.02^{d}	76.17 ± 0.78^{ef}	16.47 ± 0.91^{b}	2.44 ± 0.12^{d}
10–15	0.21 ± 0.01^{bcd}	10.10 ± 0.68^{bc}	329.89 ± 13.25^{d}	14.74 ± 0.07^{c}	2.63 ± 0.001^{e}	5.13 ± 0.01^{d}	0.27 ± 0.00^{a}	0.31 ± 0.02^{ab}	75.27 ± 2.16^{ef}	16.68 ± 0.69^{b}	2.35 ± 0.08^{d}
25–30	0.18 ± 0.01^{a}	10.64 ± 0.50^{cd}	249.16 ± 10.67^{bc}	17.59 ± 0.08^{e}	2.62 ± 0.001^{d}	3.38 ± 0.01^{a}	0.38 ± 0.02^{b}	0.30 ± 0.02^{ab}	72.73 ± 1.00^{cde}	20.07 ± 0.58^{c}	3.14 ± 0.14^{e}
40–60	0.18 ± 0.01^{ab}	12.98 ± 0.72^{e}	310.07 ± 18.91^{d}	21.45 ± 0.12^{f}	2.61 ± 0.000^{c}	4.62 ± 0.04^{c}	0.37 ± 0.01^{b}	0.32 ± 0.01^{ab}	70.23 ± 0.54^{bcd}	20.30 ± 0.65^{c}	4.16 ± 0.06^{f}
60–80	0.18 ± 0.02^{ab}	16.93 ± 1.82^{f}	205.24 ± 13.86^{a}	25.48 ± 0.28^{g}	2.58 ± 0.002^{a}	5.05 ± 0.14^{d}	0.50 ± 0.02^{c}	0.42 ± 0.01^{c}	59.04 ± 1.37^{a}	30.15 ± 1.34^{f}	4.83 ± 0.08^{g}
F	6.69	33.85	64.03	2073.70	502.35	94.40	96.16	363.81	32.39	133.17	602.32
p	<0.05	<0.05	<0.05	<0.05	<0.05	<0.05	<0.05	<0.05	<0.05	<0.05	<0.05

Abbreviations: V_t—the total pore volume; S_{MIP}—the total pore area; D_{av}—average pore diameter; SSA—specific surface area; D—surface fractal dimension.

Cumulative intrusion curves are shown in Figure 2A,C. The curves are plotted from the largest pore diameter on the *X*-axis so that the course of mercury intrusion can be followed upward from the lowest pressure. Regardless of the soil profile, the curves had a similar sigmoidal shape, characterized by one steep intrusion step, which ends with a more or less distinct plateau at a relatively small pore diameter (<0.03 µm). The pore diameter at which the plateau is reached depends slightly on the soil profile layer. Regardless of the analyzed soil profile, the largest intrusion is observed for samples from a 0–5 cm depth. In the case of Profile 1, the curve obtained for the top layer is shifted towards pores with a larger diameter. The corresponding differential pore size distribution for the studied soil profile layers is presented in Figure 2B,D. The analysis of these curves allowed for pore diversity assessment and visualization of the main distribution peaks. Generally, all PSD curves were unimodal, with a characteristic peak ranging from about 0.03 to about 1 µm. This suggests that the samples from the particular layers were relatively homogeneous and contained particles/aggregates of similar size and shape. Only in the case of Profile 1 and the 0–5 cm soil layer, the main peak was slightly wider, indicating the presence of pores of a larger diameter. Ultramicropores were the dominant pore group in both Profile 1 and Profile 2. With increasing depth of the soil profiles, the amount of ultramicropores decreased in favor of cryptopores. Cryptopores accounted for 14 to 21% and 16 to 30% of the total pore volume in Profiles 1 and 2, respectively. The other pore groups were marginal and did not exceed 5% of the total pore volume.

As a result of the potentiometric titration of the samples, the distribution functions of the apparent dissociation constant f(pKa) were designated (Figure 3). They assess the participation of functional groups with different acidity (pKa) to all negatively dissociating functional groups. At low pKa, strongly acidic carboxyl functional groups (COOH) dissociate, while at high pKa, weakly acidic groups (e.g., OH) also reveal the charge. Above

the pK 4.5, the obtained functions are close to the parabola shape with a characteristic minimum at pKa from 6.5 to 7. Dominant surface functional groups represent strongly acidic groups that dissociate at pH 4.75 and weakly acidic groups that dissociate at pH 9–10 (Figure 3). The distribution does not differ significantly in the samples taken from different depths of Profile 1, which can be explained by the low variation in the SOC (0.74 ± 0.05%) in the 10–80 cm layer. There are slightly more weakly acidic groups in the samples taken from the surface layer. The distribution of functional groups in Profile 2 is similar but with greater variation between individual depths. There are also fewer dissociating groups at pH below 4 compared to Profile 1.

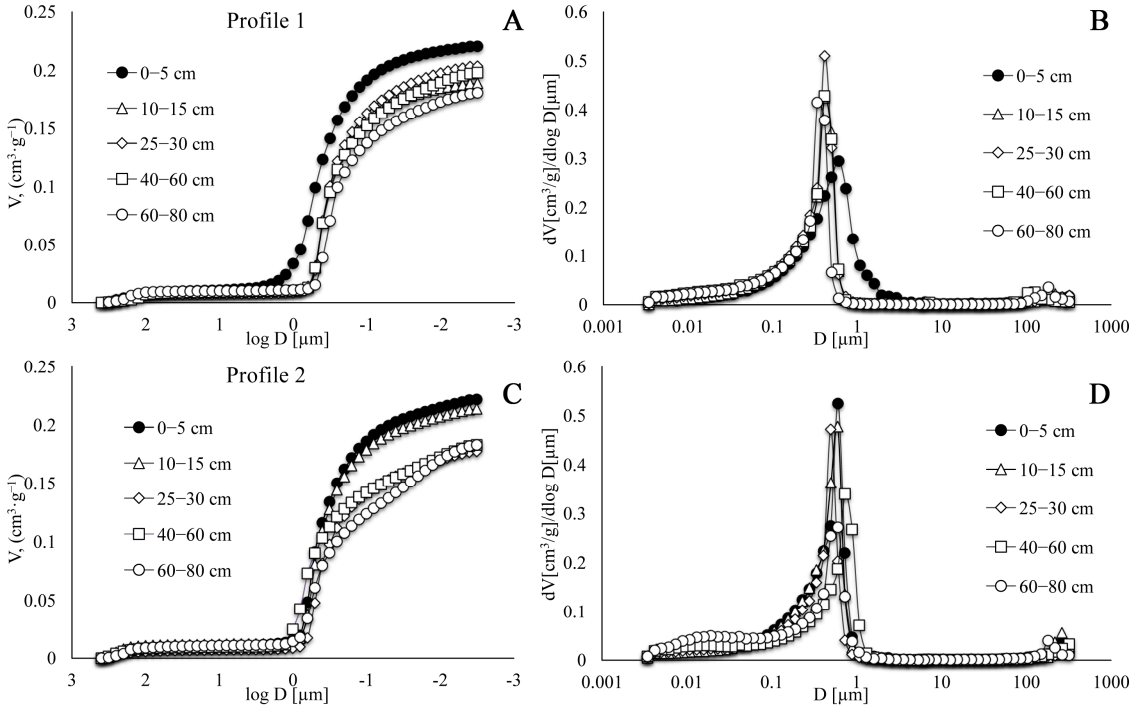


Figure 2. Mercury intrusion porosimetry data in the form of cumulative (**A**,**C**) and differential curves (**B**,**D**) obtained for two soil profiles and different soil depths.

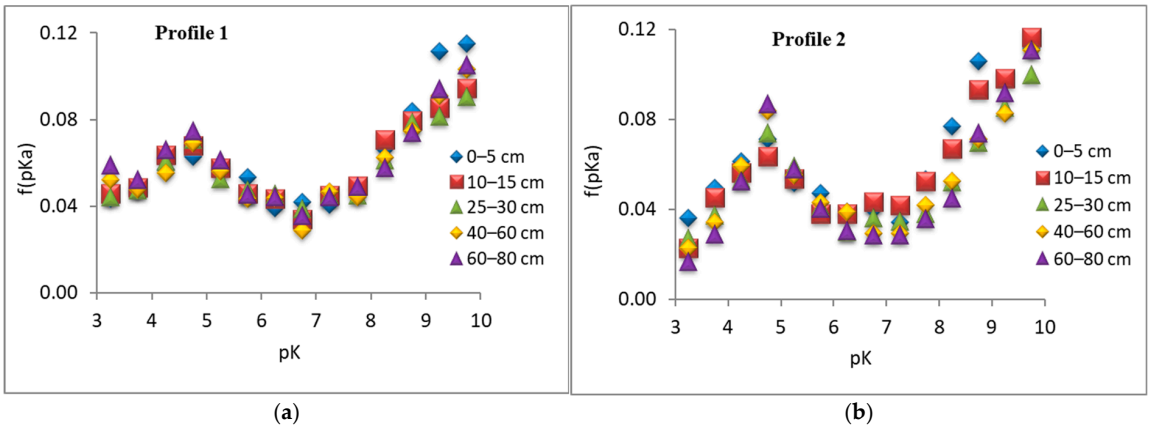
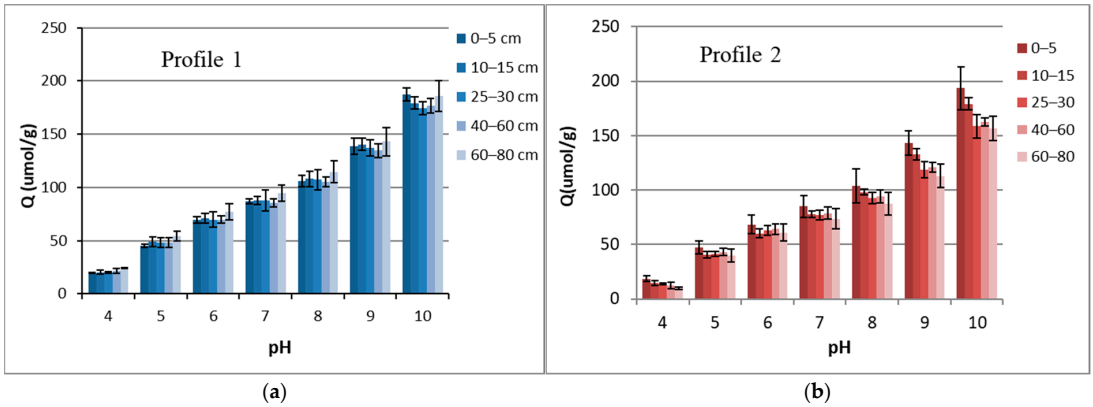


Figure 3. Apparent surface dissociation constant distribution functions (f(pKa)) obtained for soil Profile 1 (**a**) and Profile 2 (**b**) and different soil depths. Data represent mean values from three independent measurements conducted at 25 °C, under the N_2 atmosphere, across a pH titration range of 3–10.

Figure 4 presents the results of the cumulative change in the negative surface charge. The Q values increase with increasing pH due to the dissociation of the next protons from the

functional groups. A significant increase in charge is observed between pH 4 and 5, indicating that most of the functional groups generate the charge at this pH. For Profile 1, the differences between samples from different depths are not significant, with a certain increase in surface charge observed in the deeper layers. More noticeable changes are observed in Profile 2. The surface charge decreases with depth, probably due to the decrease in organic matter content. These differences in the soil profile are well illustrated by the surface charge at pH 10 (Figure 5). At this pH, all negatively dissociating groups are already dissociated, revealing almost total negative charge. It can be assumed that the value of this charge indicates the number of monovalent cations that soil can retain/exchange. In Profile 2, the highest values of the total charge are found in the top layer and decrease with depth.



(**a**) (**b**)

Figure 4. Distribution of surface charge (Qv) calculated from the titration curves of soil Profile 1 (**a**) and Profile 2 (**b**). Data represent mean values with standard deviation bars from three independent measurements conducted at 25 °C, under the N_2 atmosphere, across a pH titration range of 3–10.

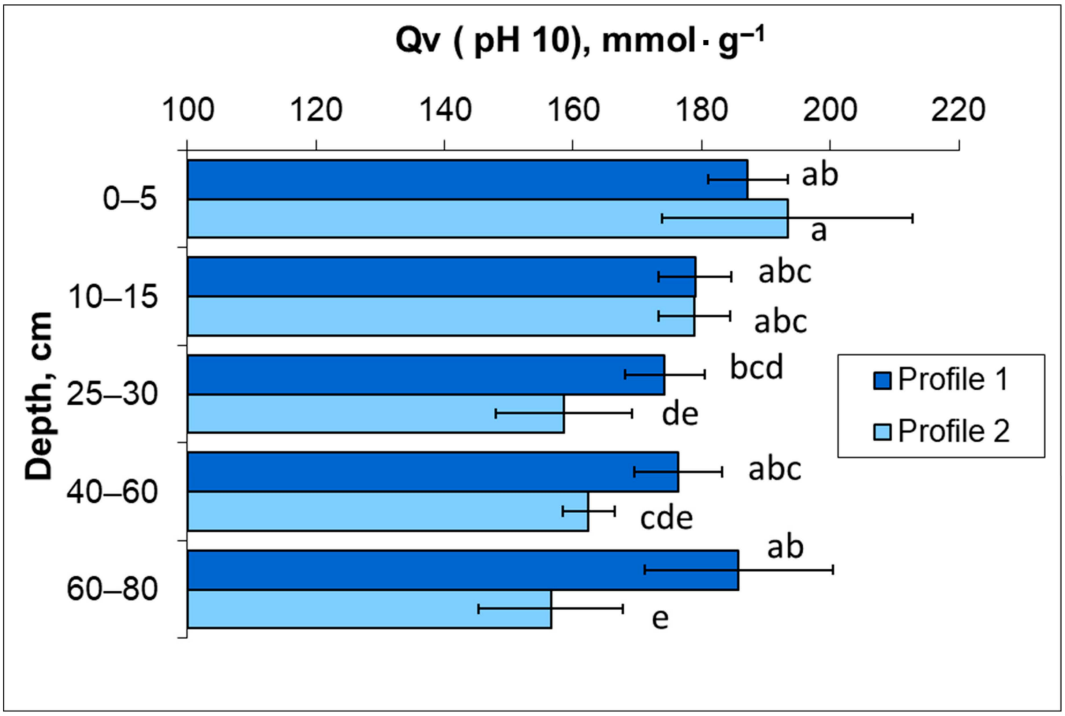


Figure 5. Average total variable surface charge (Qv) along the depth (cm) of soil profiles. Data represent mean values at pH 10 with standard deviation bars from three independent measurements conducted at 25 °C, under the N2 atmosphere. The same letter (a-e) means no significant differences between the values at the level of significance $\alpha = 0.05$, one-way ANOVA, and Tukey's HSD test.

The correlation analysis between the determined physicochemical parameters established a strong positive correlation between pH and the degree of base saturation (r = 0.96) and a negative correlation with the total acidity ($H_{8.2}$) (r = −0.96) (Table 7). The total surface charge Qv, determined by potentiometric titration at pH 10, correlated (r = 0.90) with the capacity of the weakly acidic ion exchanger (CEC_A) (Table 7).

Table 7. Correlations between physicochemical properties. Stars denote confidence level of significance of correlations (single star—90%, two stars—95%, and three stars—99%).

	Qv	SOC	pH	CEC	CEC_{SA}	CEC_A	Exch.$H_{8.2}$	Exch. Al	Base Saturation
Qv	1								
SOC	0.86 **	1							
pH in H_2O	−0.74 *	−0.68	1						
$T_{8.2}$≡CEC	0.46	0.41	0.14	1					
CEC_{SA}	−0.32	−0.33	0.76	0.65	1				
CEC_A	0.90 ***	0.85 **	−0.83 **	0.21	−0.61	1			
Exch. $H_{8.2}$	0.77 **	0.77 **	−0.96 ***	−0.07	−0.77 **	0.92 ***	1		
Exch. Al	0.48	0.58	−0.88 ***	−0.39	−0.85 **	0.69 *	0.91 ***	1	
Base saturation	−0.64	−0.65	0.96 ***	0.29	0.89 ***	−0.83 **	−0.98 ***	−0.96 ***	1

Qv—Average total variable surface charge.

The average amount of agronomically valuable aggregates (0.25–10 mm) is slightly over 50% (57 and 53%, respectively, in Profiles 1 and 2) (Figure 6). The distribution of aggregates and the mean weighted diameter (MWD) of aggregates below 10 mm also do not differ significantly within soil profiles and depths. The amount of clods (>10 mm) is significant. The water resistance of soil aggregates constituting the composite sample (size 0.25–10 mm) is very low below the surface layer (Figure 7).

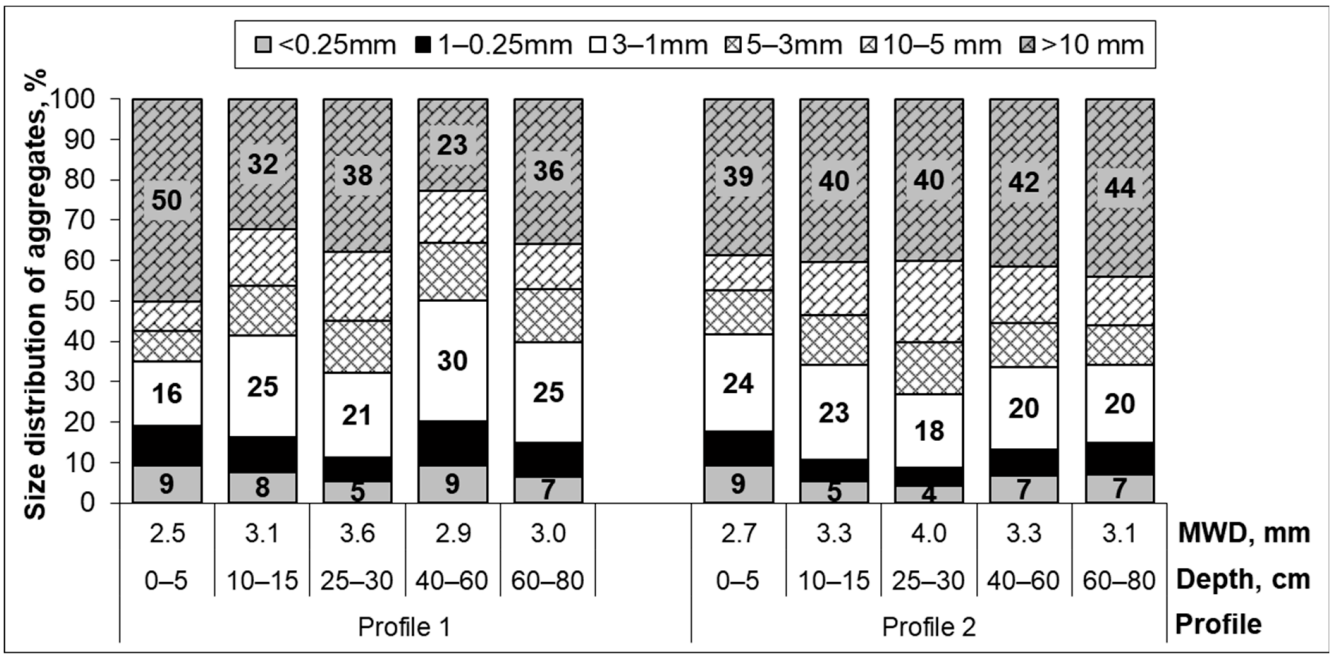


Figure 6. Aggregate size distribution and mean weight diameter (MWD) of dry aggregates.

The soil particle density (Ds) is relatively high, from 2.75 to 2.78 g · cm^{-3} in Profile 1 and from 2.71 to 2.80 g · cm^{-3} in Profile 2, which can be explained by the HM content (Table 8). The bulk density (Db) is low in the surface soil layer, then increases with depth, and the total porosity correspondingly decreases with depth, which can be explained by a decrease in the organic matter content. The hygroscopic moisture content at 75% relative humidity (pF 5.6) and the wilting point (pF 4.2) increase slightly with depth due to the

increase in clay. The water retention capacity at pF 2.0 is high only in the 0–5 cm soil surface layer (Table 8).

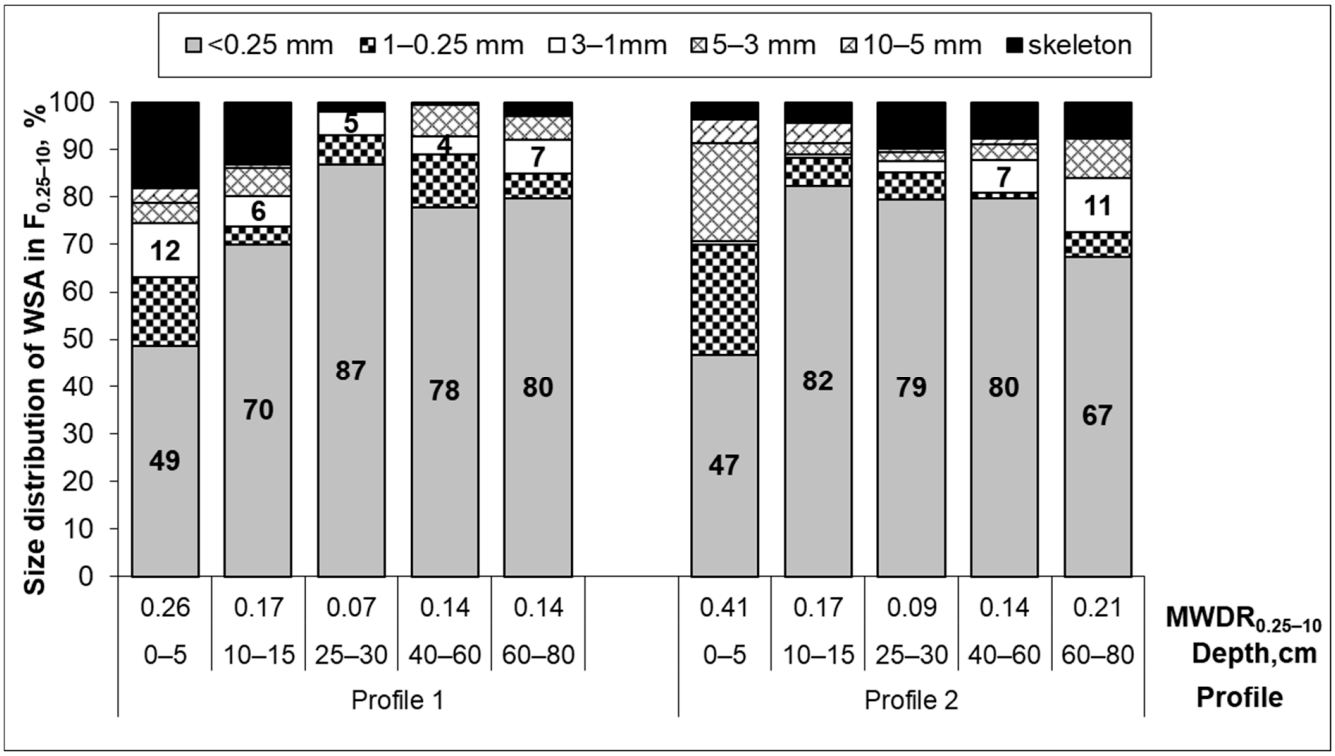


Figure 7. Size distribution of water-stable aggregates (WSAs) in the composite sample ($F_{0.25–10}$) and mean weight diameter ratio before and after wet sieving ($MWDR_{0.25–10}$).

Table 8. Soil physical properties. $MWDR_{1–3}$—mean weight diameter ratio of aggregate size 1–3 mm before and after wet sieving, Db—soil bulk density, Ds—particle density, Pt—total porosity, and soil water retention (W) at suctions pF 2.0 (field capacity), 4.2 (wilting point), and 5.6 (hygroscopic water content).

Depth cm	$MWDR_{1–3}$	Db g cm^{-3}	Ds g·cm^{-3}	Pt %*v*/*v*	$W_{2.0}$ % *w*/*w*	$W_{4.2}$ % *w*/*w*	$W_{5.6}$ % *w*/*w*
Profile 1							
0–5	0.43 ± 0.02 ^{a*}	1.07 ± 0.18 ^{a}	2.75	61.3 ± 6.6 ^{a}	38.4 ± 5.1 ^{a}	9.2 ± 0.1 ^{a}	3.04 ± 0.04 ^{b}
10–15	0.18 ± 0.05 ^{b}	1.42 ± 0.06 ^{b}	2.77	48.5 ± 2.1 ^{b}	23.4 ± 0.7 ^{de}	9.3 ± 0.1 ^{a}	2.78 ± 0.03 ^{a}
25–30	0.17 ± 0.02 ^{bc}	1.53 ± 0.01 ^{bc}	2.76	44.6 ± 0.4 ^{bc}	25.3 ± 0.3 ^{cd}	10.9 ± 0.0 ^{c}	3.01 ± 0.03 ^{b}
40–60	0.15 ± 0.04 ^{bcd}	n.d. **	2.78	n.d.	n.d.	12.2 ± 0.0 ^{f}	3.35 ± 0.02 ^{c}
60–80	0.15 ± 0.03 ^{bc}	n.d.	2.77	n.d.	n.d.	11.6 ± 0.2 ^{e}	3.57 ± 0.02 ^{d}
Profile 2							
0–5	0.10 ± 0.01 ^{d}	1.18 ± 0.02 ^{a}	2.71	56.6 ± 0.7 ^{a}	32.9 ± 1.3 ^{b}	11.0 ± 0.4 ^{c}	3.72 ± 0.05 ^{e}
10–15	0.12 ± 0.01 ^{cd}	1.43 ± 0.09 ^{b}	2.73	47.6 ± 3.2 ^{b}	26.6 ± 1.2 ^{c}	11.3 ± 0.1 ^{d}	3.63 ± 0.03 ^{d}
25–30	0.19 ± 0.03 ^{b}	1.61 ± 0.08 ^{c}	2.77	41.9 ± 2.9 ^{c}	21.2 ± 1.2 ^{e}	10.5 ± 0.1 ^{b}	3.57 ± 0.10 ^{d}
40–60	0.16 ± 0.04 ^{bc}	n.d.	2.78	n.d.	n.d.	11.4 ± 0.2 ^{de}	3.81 ± 0.02 ^{f}
60–80	0.16 ± 0.02 ^{bc}	n.d.	2.80	n.d.	n.d.	13.1 ± 0.1 ^{g}	3.97 ± 0.03 ^{g}
F	27.86	22.36		20.8	36.5	162.35	244.93
p	<0.0001	<0.0001		<0.0001	<0.0001	<0.0001	<0.0001

* The same upper letter (a–g) means no significant differences between the values at the level of sig-nificance $\alpha = 0.05$, one-way ANOVA, and Tukey's HSD test. ** n.d.—not determined.

The correlation coefficients between the heavy metal concentrations and physicochemical and physical parameters are presented in Table 9. The Cu, which has the highest soil loading (except for the case of high Pb data point), significantly ($p < 0.001$) correlates with

most physicochemical properties, except the total CEC. This is explained by the opposite reaction of Cu to CEC^{SA} and CEC^{A}. The same acidification role has the Zn concentrations. The high correlations with SOC in the case of Zn, Cu, Pb, and As can be attributed to the formation of organo-mineral complexes. The observed significant negative correlations of As, Pb, and Zn with the clay content and specific surface area (SSA) are an indication of structural changes in the contaminated soil, which is also in agreement with other studies [11]. These results are supported by the observed changes in the pore size distribution, obtained by the MIP, when the HMs increase. A decrease in the smallest pores (cryptopores and pores < 7 nm) and an increase in ultra- and micropores are observed. The water stability of the single aggregate fraction ($MWDR_{1–3}$) correlates with the content of the micropores (r = 0.80), which can explain the relation of As, Pb, and Zn with the $MWDR_{1–3}$. The presence of larger aggregates (size of 3–5 and 5–10 mm) in the composite sample explains the lower water stability of the composite sample ($MWDR_{0.25–10}$) as the forces of the binding agents between them are weaker.

Table 9. Correlations between the heavy metal concentrations and physicochemical and physical parameters. Stars denote confidence level of significance of correlations (single star—90%, two stars—95%, and three stars—99%).

	As	Cd	Cu	Pb	Zn
$T_{8.2} \equiv CEC$	0.49	−0.03	0	0.41	0.28
CEC_{SA}	0	0.31	−0.70 **	0.09	−0.28
CEC_{A}	0.51	−0.42	0.90 ***	0.31	0.66 **
Exch. $H_{8.2}$	0.47	−0.39	0.91 ***	0.35	0.70 **
Exch. Al	0.41	−0.27	0.81 ***	0.37	0.64 **
Base saturation	−0.33	0.36	−0.88 ***	−0.24	−0.61 *
Qv (surface charge)	0.5	−0.22	0.79 ***	0.34	0.66 **
SOC	0.76 *	−0.17	0.87 ***	0.68 **	0.89 ***
pH in H_2O	−0.3	0.37	−0.83 ***	−0.23	−0.64 **
EC	−0.17	0.49	−0.61 *	−0.13	−0.52
sand (2–0.063 mm)	0.67 **	−0.3	0.3	0.58 *	0.41
clay (<0.002 mm)	−0.87 ***	0.27	−0.57 *	−0.81 ***	−0.74 **
MWDR ($F_{0.25–10\,mm}$)	0.56 *	−0.07	0.44	0.30	0.31
MWDR ($F_{1–3\,mm}$)	0.84 ***	−0.01	0.32	0.95 ***	0.75 **
V_t (total pore volume, MIP)	0.63 *	0.02	0.82 ***	0.51	0.71 **
D_{av} (average pore diameter)	0.77 ***	0.18	0.58 *	0.69 **	0.64 **
SSA (specific surface area)	−0.53	0.37	−0.86 ***	−0.49	−0.79 ***
D (surface fractal dimension)	0.69 **	−0.27	0.76 **	0.59 *	0.70 **
Macropores (>75 μm)	−0.18	0.42	−0.25	−0.19	−0.17
Mesopores (75–30 μm)	0.65 **	−0.18	0.15	0.64 **	0.49
Micropores (30–5 μm)	0.95 ***	−0.01	0.45	0.92 ***	0.78 ***
Ultramicropores (5–0.1 μm)	0.55 *	−0.23	0.75 **	0.46	0.62 *
Cryptopores (0.1–0.007 μm)	−0.58 *	0.14	−0.69 **	−0.48	−0.59 *
Pores < 7 nm	−0.53	0.36	−0.91 ***	−0.48	−0.79 ***
$W_{4.2}$ (wilting point)	−0.60 *	0.41	−0.66 **	−0.55	−0.63 *
$W_{5.6}$ (hygroscopic water)	−0.36	0.36	−0.70 **	−0.39	−0.67 **

There is a lack of thermal conductivity data for contaminated soils [32], despite the information being needed to predict the temperature rise and energy consumption during the thermal remediation process for removal of contaminants by heating the soil. The thermal conductivity (λ) of the soil, measured at different matrix potentials, increases with depth due to an increase in the bulk and particle density of the soil (Figure 8). The difference between the 0–5 cm surface and 10–15 cm subsurface soil layer is significant, while the differences in thermal conductivity between profiles measured at the same depths are not large. The RMSEs of the predicted λ by the de Vries' model were in the range 0.039–0.0479 W $m^{-1} \cdot K^{-1}$.

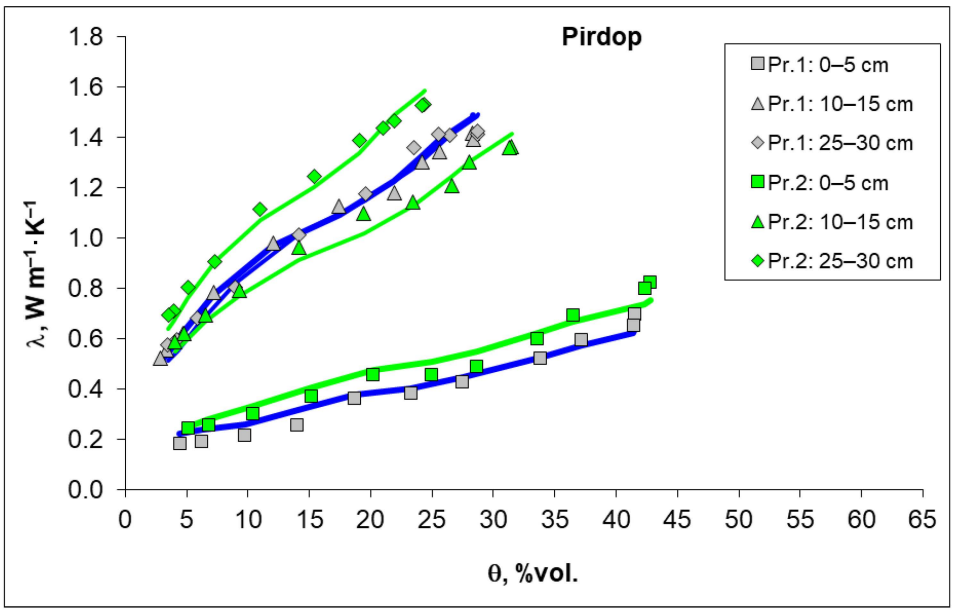


Figure 8. Measured (symbols) and modeled (lines) soil thermal conductivity λ by de Vries [21] as function of volumetric water content (θ).

4. Conclusions

Data on physical, physicochemical, mineralogical, and thermal properties were obtained from the soil profiles under a non-cultivated area located at different distances from the Aurubis-Pirdop Copper smelter, which is a source of aerosol pollution with heavy metals. Against the background of clearly expressed differences in the amount and distribution of concentrations by depth in the two profiles, especially of Cu and Pb, a large set of soil parameters has been measured and statistically analyzed to establish a connection with the Cu, Zn, Pb, As, and Cd concentrations. Depending on the HM speciation, the correlations are established with the SOC and most of the physicochemical parameters. It can be concluded that the HMs impact the clay content, specific surface area, distribution of pores, and the water stability of soil aggregates of 1–3 mm size to varying degrees.

Author Contributions: Conceptualization, M.K. and P.B.; methodology, M.K., P.B., K.S. and M.B.; formal analysis, M.K., P.B., K.S. and K.D.; investigation, M.K., P.B., K.S., V.K., K.D. and M.B.; resources, M.K., P.B. and K.S.; data curation, M.K., P.B., K.S. and M.B.; writing—original draft preparation, M.K., P.B., K.S. and K.D.; writing—review and editing, M.K., P.B. and K.S.; visualization, M.K., P.B., K.S. and K.D.; supervision, M.K.; project administration, M.K.; funding acquisition, M.K. All authors have read and agreed to the published version of the manuscript.

Funding: This research was funded by the Bulgarian National Science Fund under grant agreement DN16/11 (project "Thermal properties of soils at different land use and melioration").

Data Availability Statement: All data analyzed during this study are included in this.

Conflicts of Interest: The authors declare no conflicts of interest.

Abbreviations

The following abbreviations are used in this manuscript:

MPC	Maximum permissible concentration
IC	Intervention concentration—according to [16]
WSA	Water-stable aggregate
HM	Heavy metal
MIP	Mercury intrusion porosimetry

SOC	Soil organic carbon content
EC	Electrical conductivity
CEC	Total sum of exchange cations
CEC_{SA}	Cation-exchange capacity of soil strongly acidic ion exchanger
CEC_A	CEC of slightly acidic ion exchanger

References

1. Micó, C.; Recatalá, L.; Peris, M.; Sánchez, J. Assessing Heavy Metal Sources in Agricultural Soils of an European Mediterranean Area by Multivariate Analysis. *Chemosphere* **2006**, *65*, 863–872. [CrossRef]
2. Violante, A.; Cozzolino, V.; Perelomov, L.; Caporale, A.G.; Pigna, M. Mobility and Bioavailability of Heavy Metals and Metalloids in Soil Environments. *J. Soil Sci. Plant Nutr.* **2010**, *10*, 268–292. [CrossRef]
3. Tóth, G.; Hermann, T.; Da Silva, M.R.; Montanarella, L. Heavy Metals in Agricultural Soils of the European Union with Implications for Food Safety. *Environ. Int.* **2016**, *88*, 299–309. [CrossRef]
4. Rajendran, S.; Priya, T.A.K.; Khoo, K.S.; Hoang, T.K.A.; Ng, H.-S.; Munawaroh, H.S.H.; Karaman, C.; Orooji, Y.; Show, P.L. A Critical Review on Various Remediation Approaches for Heavy Metal Contaminants Removal from Contaminated Soils. *Chemosphere* **2022**, *287*, 132369. [CrossRef]
5. Ali, H.; Khan, E.; Ilahi, I. Environmental Chemistry and Ecotoxicology of Hazardous Heavy Metals: Environmental Persistence, Toxicity, and Bioaccumulation. *J. Chem.* **2019**, *2019*, 6730305. [CrossRef]
6. Angon, P.B.; Islam, M.S.; Kc, S.; Das, A.; Anjum, N.; Poudel, A.; Suchi, S.A. Sources, Effects and Present Perspectives of Heavy Metals Contamination: Soil, Plants and Human Food Chain. *Heliyon* **2024**, *10*, e28357. [CrossRef] [PubMed]
7. Mohammad, S.J.; Ling, Y.E.; Halim, K.A.; Sani, B.S.; Abdullahi, N.I. Heavy Metal Pollution and Transformation in Soil: A Comprehensive Review of Natural Bioremediation Strategies. *J. Umm Al-Qura Univ. Appll. Sci.* **2025**, *11*, 528–544. [CrossRef]
8. Wijngaard, R.R.; Van Der Perk, M.; Van Der Grift, B.; De Nijs, T.C.M.; Bierkens, M.F.P. The Impact of Climate Change on Metal Transport in a Lowland Catchment. *Water Air Soil Pollut.* **2017**, *228*, 107. [CrossRef]
9. Kicińska, A.; Pomykała, R.; Izquierdo-Diaz, M. Changes in Soil pH and Mobility of Heavy Metals in Contaminated Soils. *Eur. J. Soil Sci.* **2022**, *73*, e13203. [CrossRef]
10. Li, Q.; Wang, Y.; Li, Y.; Li, L.; Tang, M.; Hu, W.; Chen, L.; Ai, S. Speciation of Heavy Metals in Soils and Their Immobilization at Micro-Scale Interfaces among Diverse Soil Components. *Sci. Total Environ.* **2022**, *825*, 153862. [CrossRef]
11. Zhang, G.; Liu, T.; Li, H.; Wang, Z.; Huang, X.; Yi, X.; Yan, D. Experimental Study on the Effects of Heavy Metal Pollution on Soil Physical Properties and Microstructure Evolution. *Appl. Sci.* **2024**, *14*, 2022. [CrossRef]
12. Deng, A.; Wang, L.; Chen, F.; Li, Z.; Liu, W.; Liu, Y. Soil Aggregate-Associated Heavy Metals Subjected to Different Types of Land Use in Subtropical China. *Glob. Ecol. Conserv.* **2018**, *16*, e00465. [CrossRef]
13. Atanassova, I.; Benkova, M.; Nenova, L.; Simeonova, T.; Harizanova, M. Sources of Metals, Metalloids and Non-Metals in Surface Horizons of Soils near Aurubis-Pirdop Copper Smelter in Bulgaria. *Bulg. J. Agric. Sci.* **2024**, *30*, 561–567.
14. Kancheva, V.; Dinev, N.; Gadjalska, N. Risk Assessment of Copper Contamination in Soil and Surface Water in Topolnitsa River Catchment. *Bulg. J. Soil Sci. Agrochem. Ecol.* **2018**, *52*, 3–9.
15. Benkova, M.; Atanassova, I. Effectiveness of Lime and Glauconite-Phosphorite Containing Organo-Mineral Ameliorants in Heavy-Metal-Contaminated Soils. In *Phosphate in Soil: Interaction with Microelements, Radionuclides and Heavy Metal*; CRC Press: Boca Raton, FL, USA, 2015; pp. 293–320.
16. Dimitrov, D.; Markov, E. Comparative Study on the Trends in the Soil Formation Processes in Situation of Aerosol Input of Cu, Zn, Pb, As, SO_2. *Soil Sci. Agrochem. Ecol.* **2000**, *35*, 11–14.
17. Kercheva, M.; Paparkova, T.; Dimitrov, E.; Doneva, K.; Nedyalkova, K.; Perfanova, J.; Sechkova, R.; Velizarova, E.; Glushkova, M. Soil Structure Characteristics in Three Mountainous Regions in Bulgaria Under Different Land Uses. *Forests* **2025**, *16*, 1065. [CrossRef]
18. *Soil Quality—Determination of Particle Size Distribution in Mineral Soil Material—Method by Sieving and Sedimentation*; ISO: Geneva, Switzerland, 2020; pp. 11277–12020.
19. Revut, I.B. *Methods of Soil Structure Investigations*; Kolos Press: Leningrad, Soviet Union, 1969.
20. Six, J.; Elliott, E.T.; Paustian, K. Soil Structure and Soil Organic Matter II. A Normalized Stability Index and the Effect of Mineralogy. *Soil Sci. Soc. Am. J.* **2000**, *64*, 1042–1049. [CrossRef]
21. de Vries, D.A. Thermal Properties of Soils. In *Physics of Plant Environment*; van Wijk, W.R., Ed.; North-Holland Publishing Company: Amsterdam, The Netherlands, 1963; pp. 210–235.
22. Filcheva, E.; Tsadilas, C. Influence of Cliniptilolite and Compost on Soil Properties. *Commun. Soil Sci. Plant Anal.* **2002**, *33*, 595–607. [CrossRef]
23. Kononova, M.M. *Soil Organic Matter. Its Nature, Properties and Methods of Study*; USSR Academy of Sciences: Moscow, Soviet Union, 1963.

24. Ganev, S.; Arsova, A. Methods for Determining the Strongly Acid and Weakly Acid Cation Exchange in Soil. *Soil Sci. Agrochem.* **1980**, *15*, 22–33.
25. Skic, K.; Boguta, P.; Sokołowska, Z. Analysis of the Sorption Properties of Different Soils Using Water Vapour Adsorption and Potentiometric Titration Methods. *Int. Agrophys.* **2016**, *30*, 369–374. [CrossRef]
26. Cameron, K.C.; Buchan, G.D. Porosity and Pore Size Distribution. *Encycl. Soil Sci.* **2006**, *2*, 1350–1353.
27. Decree No. 3 from 1st August 2008 for Standards of Acceptable Content of Harmful Substances in the Soil. State Gazette, Issue 71. 12 August 2008, p. 75. Available online: https://dv.parliament.bg/DVWeb/showMaterialDV.jsp?idMat=7670 (accessed on 29 June 2025).
28. Atanassov, I. New Bulgarian Soil Pollution Standards. *Bulg. J. Agric. Sci.* **2007**, *14*, 68–75. Available online: https://agrojournal.org/14/01-08-08.pdf (accessed on 29 June 2025).
29. van Lynden, G.W.J. *Guidelines for the Assessment of Soil Degradation in Central and Eastern Europe (SOVEUR). Report 97/08b (Revised Edition)*; ISRIC: Wageningen, The Netherlands, 2000.
30. Ministry of the Environment. *Finland Government Decree on the Assessment of Soil Contamination and Remediation Needs*; Ministry of the Environment: Helsinki, Finland, 2007; p. 214. Available online: https://www.finlex.fi/en/legislation/translations/2007/eng/214 (accessed on 11 September 2025).
31. Ganev, S. *Modern Soil Chemistry*; Science and Art: Sofia, Bulgaria, 1990.
32. Wu, Y.-H.; Wu, Y.-F.; Fan, L.-W.; Yu, Z.-T.; Khodadadi, J.M. Thermal Conductivity of Soil: A Review on the Vast Experimental Data and Predictive Models. *Int. J. Therm. Sci.* **2025**, *208*, 109486. [CrossRef]

Disclaimer/Publisher's Note: The statements, opinions and data contained in all publications are solely those of the individual author(s) and contributor(s) and not of MDPI and/or the editor(s). MDPI and/or the editor(s) disclaim responsibility for any injury to people or property resulting from any ideas, methods, instructions or products referred to in the content.